V European Conference on Computational Fluid Dynamics
ECCOMAS CFD 2010
J. C. F. Pereira and A. Sequeira (Eds)
Lisbon, Portugal,14-17 June 2010

OPTIMAL DISTURBANCES AND RECEPTIVITY IN THREE-DIMENSIONAL BOUNDARY LAYERS

David Tempelmann*, Ardeshir Hanifi†,* and Dan S. Henningson*

*KTH Mechanics, Linné Flow Center, SE-100 44 Stockholm, Sweden
e-mail: {david, henning}@mech.kth.se
†Swedish Defence Research Agency, FOI, SE-164 90 Stockholm, Sweden
e-mail: ardeshir.hanifi@foi.se

Key words: Optimal disturbances, receptivity, three-dimensional boundary layers, cross-flow disturbances, parabolised stability equations

Abstract. *A new method representing a modification of the well-known parabolised stability equations (PSE) is introduced. Compared to the classical form of the PSE this modification makes it possible to study more general disturbances. Hence, these modified PSE allow to efficiently predict the spatial evolution of both non-modal and modal disturbances in three-dimensional boundary layers.*
Employing adjoint-based optimisation, the modified PSE are used to compute spatial optimal disturbances which experience maximum energy amplification and therefore represent the worst case scenario. It is shown how these optimal disturbances can be used to approximate the response of a boundary layer to free-stream vorticity. Further, it is illustrated how the modified PSE may be employed directly to study receptivity to free-stream vorticity in 3D boundary layers.

1 Introduction

Modelling the transition process of boundary layers to get to know the location of transition from laminar to turbulent flow is of great interest for the design of airplane wings. The transition process of boundary layers is mainly characterised by three stages. These are receptivity, growth and breakdown of disturbances. Receptivity is associated with the birth of disturbances inside a boundary layer which is exposed to an external disturbance environment. Acoustic perturbations, surface roughness or free-stream turbulence represent such external disturbances which are filtered by the boundary layer. The excited disturbances grow while evolving downstream. Initially this growth may be described by linear theory. Once the disturbances reach a certain amplitude nonlinear effects will lead to amplitude saturation promoting the growth of secondary instabilities which will quickly cause the flow to transition from a laminar to a turbulent state.
A complete model of the transition process which can reliably predict the location of transition should incorporate all three stages. Semi-empirical transition prediction tools, which are in common use today, are based on the linear amplification of modal disturbances only and disregard the disturbance environment. However, the latter is known to greatly influence the transition process of the boundary layer.
[1] performed experiments to study the disturbance development in three-dimensional boundary layers in different wind tunnels. The different environmental conditions were found to strongly influence the disturbance development inside the boundary layer. In a review [2] reports that stationary crossflow modes dominate in three-dimensional boundary layers exposed to low levels of free-stream turbulence whereas travelling disturbances dominate in high turbulence level environments. The latter statement was numerically verified by [3] who study the transition of a Falkner-Skan-Cooke boundary layer exposed to free-stream turbulence and localised surface roughness. The simulations show that stationary crossflow modes dominate unless the turbulence intensity of the incoming flow is larger than 0.5%.
One consequence of these findings is that test results for airplane wings obtained in wind tunnels might not be readily transferred to free flight conditions where the levels of free-stream turbulence are relatively low. Hence, both experimental and numerical studies show that a detailed knowledge of the disturbance environment is necessary to be able to prescribe the disturbance development inside the boundary layer. Once the external disturbances are known the task is to identify the disturbances which are excited inside the boundary layer. However, getting information about the external disturbance environment, in particular in the free-stream, is not trivial.
If the external disturbance field is not known it makes sense to consider the worst case scenario as is outlined by [4]. This implies finding those initial disturbances experiencing maximum energy amplification, the so-called *optimal disturbances*. These have been extensively studied for two-dimensional boundary layers over the past few years (see e.g. [5, 6, 7, 8]). Substantial energy growth of streak-like disturbances has been observed

in *sub-critical* boundary layers which are stable with respect to modal disturbances, i.e. Tollmien-Schlichting waves. This led to the expression *non-modal* growth.
However, not much work on non-modal and optimal disturbance growth has been performed for three-dimensional boundary layers. Employing a temporal approach both [10] and [11] showed that also three-dimensional boundary layers exhibit substantial non-modal growth. The disturbances subject to non-modal growth were found to be structurally similar to the modal crossflow instabilities which is in contrast to the two-dimensional case where streaks and Tollmien-Schlichting waves bear no resemblance. This led to the conclusion by [11] that non-modal growth provides the proper initial conditions for the growth of modal disturbances and may thus be related to a receptivity mechanism in three-dimensional boundary layers. To describe this process, i.e. the initiation of modal instabilities by non-modal growth, a spatial framework is needed and was introduced by [9] for incompressible three-dimensional boundary layers.
Once some information about the external disturbance environment is available we can develop models that predict the corresponding boundary layer response. The receptivity to free-stream turbulence can be modelled by considering the response of the boundary layer to free-stream vorticity. This approach has been chosen by different previous studies (see e.g. [12, 13, 14]). In the following we are going to present two methods that allow to model the receptivity of a three-dimensional boundary layer to vortical free-stream disturbances and compare respective results to the DNS performed by [14]. Both methods utilise the spatial approach developed by [9] which represents a modification of the well-known classical parabolised stability equations (PSE). While the classical PSE only allow the description of modal instabilities such as crossflow disturbances this method is used to efficiently compute the downstream development of more general initial, in this case vortex-type, disturbances.
The first method is based on the assumption that free-stream vorticity excites disturbances similar in structure to optimal disturbances in three-dimensional boundary layers. Hence, an approximation of the boundary layer response can be obtained by projecting external disturbances onto optimal disturbances. The second method bases upon directly solving the modified PSE for initial vortical free-stream disturbances.

2 Falkner-Skan-Cooke boundary layer

We study optimal disturbances and receptivity in a Falkner-Skan-Cooke (FSC) boundary layer. This type of boundary layer forming on a swept flat plate which is subject to a chordwise pressure gradient is considered to be a good model for swept-wing boundary layers. This is due to the fact that it comprises the effect of both a pressure gradient and a sweep angle. In the following we consider an FSC boundary layer which has been used by [14] to study receptivity by means of DNS. The chordwise and spanwise velocities at

the boundary layer edge are given by

$$U_\infty(x) = \frac{U_\infty^d(x)}{U_\infty^d(x_0)} = \left(\frac{x^d}{x_0^d}\right)^m \qquad V_\infty(x) = \frac{V_\infty^d(x)}{U_\infty^d(x_0)} = \tan\phi(x_0) = const, \tag{1}$$

where $m = \beta_H/(2-\beta_H)$ is related to the pressure gradient and β_H denotes the Hartree parameter which is chosen as $\beta_H = 0.333$ in the following. The sweep angle is chosen to be $\phi = 45°$ while the initial position is $x_0^d = 167\delta^*(x_0)$. The superscript d denotes dimensional quantities and δ^* represents the dimensional displacement thickness. The Reynolds number is $Re_{\delta_0^*} = U_\infty^d(x_0)\delta^*(x_0)/\nu^d = 220$ where ν^d represents the kinematic viscosity. If not marked specifically all quantities presented in the following are made non-dimensional using $\delta_0^* = \delta^*(x_0)$ and $U_\infty^d(x_0)$.

3 Methodology

In this section a modification of the well-known PSE developed by Herbert & Bertolotti (see e.g. [15]) and Dallmann & Simen (see [16]) is presented. These modified PSE, which have been introduced by [9], are used to study the spatial evolution of both modal and non-modal disturbances in three-dimensional boundary layers. They enable us to compute optimal disturbances as well as to directly determine the boundary layer response to vortical free-stream disturbances and therefore to study receptivity.

3.1 Governing equations

Our intention is to find a set of linear governing equations which describes the spatial evolution of disturbances and which is parabolic in nature. Such a system can be solved efficiently by employing marching techniques and allows for extensive parametric studies. It is derived from the Navier-Stokes equations which for incompressible flow read

$$\nabla\cdot\boldsymbol{\mathcal{U}} = 0 \tag{2a}$$

$$\frac{\partial\boldsymbol{\mathcal{U}}}{\partial t} + (\boldsymbol{\mathcal{U}}\cdot\nabla)\boldsymbol{\mathcal{U}} = -\nabla\mathcal{P} + \frac{1}{Re}\nabla^2\boldsymbol{\mathcal{U}}, \tag{2b}$$

where $Re = U_{ref}^d l_{ref}^d/\nu^d$ is the Reynolds number based on a reference velocity U_{ref}^d, a reference length l_{ref}^d and the kinematic viscosity ν^d. The superscript d denotes dimensional quantities. The pressure is denoted by $\mathcal{P}$ and $\boldsymbol{\mathcal{U}}$ denotes the velocity vector. Decomposing the flow field into a mean and a perturbation part, i.e. $\boldsymbol{\mathcal{U}} = \mathbf{U} + \mathbf{u}'$ and $\mathcal{P} = P + p'$, subtracting the equations describing the meanflow and linearising by neglecting products of perturbation quantities leads to the linear stability equations

$$\nabla\cdot\mathbf{u}' = 0 \tag{3a}$$

$$\frac{\partial\mathbf{u}'}{\partial t} + (\mathbf{u}'\cdot\nabla)\mathbf{U} + (\mathbf{U}\cdot\nabla)\mathbf{u}' = -\nabla p' + \frac{1}{Re}\nabla^2\mathbf{u}'. \tag{3b}$$

Here, mean quantities are denoted by capital letters and a prime denotes perturbation quantities. The fundamental idea behind the PSE is to decompose the disturbance into a

slowly varying and a fast oscillatory part. Accordingly, the following normal mode ansatz is made where the disturbance $\mathbf{q}'$ is decomposed into a shape function $\mathbf{q}$ and a phase function Θ. Hence,

$$\mathbf{q}'(x,y,z,t) = \mathbf{q}(x,z)\exp i\Theta(x,y,t) \tag{4}$$

$$\Theta(x,y,t) = \int_{x_0}^{x}\alpha(x')dx' + \beta y - \omega t \tag{5}$$

and $\mathbf{q} = (u,v,w,p)^T$. The coordinates (x,y,z) denote chordwise, spanwise and wall-normal directions and (u,v,w) represent the corresponding velocity components. The chordwise and spanwise wavenumbers are denoted by α and β respectively while ω represents the angular frequency. In (4) the shape function $\mathbf{q}(x,z)$ as well as the chordwise wavenumber $\alpha(x)$ are assumed to be slowly varying while the exponential part is assumed to capture the disturbance oscillations. However, the solution ansatz (4) causes an ambiguity since both the shape function $\mathbf{q}$ and the phase function Θ are functions of the chordwise coordinate x. This ambiguity is resolved by choosing α such that the assumption of a slowly varying shape function is valid. Different approaches may be chosen for different purposes. Two approaches, a classical one which is restricted to describing modal disturbances and the one employed in this study allowing for considering more general disturbances, are presented in section 3.2.
Further, a scale separation between variations in chordwise and wall-normal direction is introduced. It is assumed that variations in chordwise direction are much slower than variations in wall-normal direction. Hence, after introducing (4) into (3) chordwise derivatives and the wall-normal mean velocity component are assumed to be of order $\mathcal{O}(Re^{-1})$, i.e.

$$\frac{\partial}{\partial x}, W \rightarrow \mathcal{O}(Re^{-1}). \tag{6}$$

Identifying and neglecting all terms which are of order $\mathcal{O}(Re^{-2})$ and higher leads to a quasi parabolic equation system of the form

$$\mathbf{L}\mathbf{q} = 0 \tag{7}$$

with $\mathbf{L}$ being the linear operator

$$\mathbf{L} = \mathbf{A} + \mathbf{B}\frac{\partial}{\partial z} + \mathbf{C}\frac{\partial^2}{\partial z^2} + \mathbf{D}\frac{\partial}{\partial x}. \tag{8}$$

The operators $\mathbf{A}$, $\mathbf{B}$, $\mathbf{C}$ and $\mathbf{D}$ are defined in [9]. It should be noted that the scaling (6) is assumed to be valid for modal disturbances. In order to obtain an approximation valid for both modal and non-modal growth [17] and [9] employed a composite scaling consisting of both the PSE scaling and a scaling based on the boundary layer approximation. Performing such an analysis one additional term, uW_x, enters the wall-normal

momentum equation in (7) which was found to be important for non-modal growth by [18]. It is therefore included for the present analysis.
Introducing an initial disturbance $\mathbf{q}_0$ at a chordwise position x_0 we can solve (7) by simply marching downstream while we require solutions subject to boundary conditions

$$u = v = w = 0 \qquad \text{at} \qquad z = 0, \tag{9a}$$

$$u \to 0,\ v \to 0,\ w \to 0 \qquad \text{as} \qquad z \to \infty. \tag{9b}$$

The system (7) is only quasi parabolic in that it exhibits an inherent ellipticity which can cause numerical instabilities at small stepsizes Δx (see e.g. [19]). In order to relax this numerical instability we omit the disturbance pressure gradient p_x in the chordwise momentum equation as was proposed by [20]. By comparing to DNS, [9] showed that this term has only negligible effects on the computed results.

3.2 Choice of α

As discussed previously, the chordwise wavenumber α needs to be chosen such that the shape function $\mathbf{q}$ may be assumed to be slowly varying. Our choice of α represents the main difference to the classical PSE. In order to highlight these differences we first briefly discuss the classical approach before introducing the choice that represents an inherent part of the modified PSE and that has been employed throughout this study.

3.2.1 Classical approach

The classical approach which is employed when considering modal disturbances assumes the chordwise wavenumber to be complex and consists of an additional auxiliary function of the form

$$\int_0^\infty \mathbf{q}^H \frac{\partial \mathbf{q}}{\partial x}\, dz = 0. \tag{10}$$

This auxiliary function represents a normalisation condition on the shape function $\mathbf{q}$ and ensures that both the growth and the chordwise oscillations of the disturbance are captured by the exponential part of (4). The PSE are initiated with a local solution of the Orr-Sommerfeld/Squire equations (OSS) which provides the initial disturbance in form of $\mathbf{q}(x_0)$ and $\alpha(x_0)$. The nonlocal evolution of the modal disturbance in a non-parallel flow is then obtained by marching downstream where the auxiliary condition (10) is enforced locally at each chordwise position by employing Newton iterations or similar methods with respect to α. The required initial guess is given by the solution at the respective previous station which initially is the OSS-solution.

3.2.2 The modified PSE

The initial guess for the complex valued chordwise wavenumber required by the previous approach is not readily available for an arbitrary initial disturbance. In order to

make the PSE capable of predicting the downstream evolution of vortex-type initial disturbances we follow the approach proposed by [9]. They computed the spatial evolution of optimal disturbances based on a constant phase approach.
We choose the chordwise wavenumber to be a real-valued function such that the oscillations of the disturbance are absorbed by the exponential part of (4). If we normalise $\mathbf{q}$ by introducing a complex amplitude $A(x)$ such that $\mathbf{q}(x,z) = A(x)\hat{\mathbf{q}}(x,z)$ we can rewrite (4) according to

$$\begin{aligned} \mathbf{q}'(x,y,z,t) &= |A(x)| \exp\big(i\vartheta(x)\big)\ \hat{\mathbf{q}}(x,z) \exp\big(i\Theta(x,y,t)\big) && \text{(11a)} \\ &= |A(x)| \hat{\mathbf{q}}(x,z) \exp\big(i\hat{\Theta}(x,y,t)\big), && \text{(11b)} \end{aligned}$$

where ϑ represents the phase of the complex amplitude $A(x)$ and the phase function $\hat{\Theta}(x,y,t)$ is defined as

$$\hat{\Theta}(x,y,t) = \vartheta(x_0) + \int_{x_0}^{x} \left(\alpha(x') + \frac{\partial \vartheta}{\partial x'}\right) dx' + \beta y - \omega t. \tag{12}$$

This formulation allows to identify a new auxiliary condition. If ϑ is constant all the oscillations of $\mathbf{q}'$ are absorbed by the exponential part of (4). We thus require that

$$\vartheta(x) = const \quad \Leftrightarrow \quad \frac{\partial \vartheta}{\partial x} = 0. \tag{13}$$

We will enforce this condition globally through the following iteration procedure where k denotes the number of iterations.
1.) Choose a reasonable initial guess for the real-valued $\alpha_{k=1}(x)$ for the whole domain. In the present case a good initial guess can be obtained by assuming the line of constant phase to coincide with the external streamline. This is a good first approximation since the wave rays of streaks and crossflow modes are known to closely follow the external streamline in three-dimensional boundary layers. Note that the direction of the wavevector is normal to the line of constant phase at each position x.
2.) Solve the equation system (7) for an initial disturbance $\mathbf{q}_0$ using α_k.
3.) Compute the new candidate chordwise wavenumber according to

$$\alpha_{k+1} = \alpha_k + \frac{\partial \vartheta}{\partial x} \tag{14}$$

4.) Continue with 2.) and repeat until the disturbance energy growth is converged.

This iteration procedure ensures that $\partial\vartheta/\partial x \approx 0$ and that the periodic variations of the disturbance are almost entirely captured by the exponential part of (4). Now we can assume the shape function to be slowly varying in chordwise direction as is required for the PSE to be valid. However, since the chordwise wavenumber is chosen to be a

real number the disturbance growth is absorbed by the shape function. Strongly growing disturbances may thus fall out of reach of the equations.
A question that remains to be answered is how the complex amplitude $A(x)$ and thus the normalisation should be chosen which determine the phase function ϑ. As is outlined in [9] the phase of $\mathbf{q}$ can not be uniquely defined since different components of $\mathbf{q}$ exhibit different phases. The most reasonable choice is therefore to base ϑ on the disturbance velocity component which comprises the major part of the disturbance energy. For streak-like disturbances and crossflow modes in three-dimensional boundary layers this is the velocity component u_ϕ which is tangential to the line of constant phase (see [9]). This choice is also most appropriate here since we will consider crossflow disturbances and vortical free-stream modes where the latter will quickly evolve into streak-like disturbances due to the lift-up effect. We therefore choose $A(x) = u_{\phi,\max}$ which denotes the wall-normal maximum of u_ϕ and obtain the corresponding phase ϑ according to

$$\vartheta(x) = \arctan \frac{\Im(A(x))}{\Re(A(x))}, \tag{15}$$

where $\Im$ and $\Re$ denote the imaginary and real parts of a complex number respectively. It is just an initial region very close to the initial position where u_ϕ might not represent the most energetic flow quantity. Here initial disturbances evolve into streaks or crossflow disturbances and the phases of the initial disturbances can vary rapidly. In those cases α is determined according to the described procedure starting from the position where most of the energy $(0.9 - 0.99\%)$ is contained in u_ϕ. For the region upstream of that position, which we experienced to be very small, α is chosen constant in order to obtain rapid convergence of the results.
The approach outlined in this section which we will refer to as the modified PSE throughout this paper allows to study the evolution of all disturbances whose wave rays closely follow the external streamline. This includes streak-like and crossflow disturbances. Moreover we are now able to compute optimal disturbances by employing an appropriate optimisation and to predict the response of three-dimensional boundary layers to vortical free-stream disturbances.

The validity of the approximations made above is approved in figure 1 where we compare the downstream evolution of a crossflow mode predicted by the modified PSE and by DNS. The N-factor $N(x) = 0.5 \ln\left(E(x)/E(x_0)\right)$ as well as the growth rate $\sigma(x) = \partial N/\partial x$ are shown. Here, $E(x) = E(\mathbf{q}(x))$ denotes the energy norm of the disturbance $\mathbf{q}$ at the chordwise position x. In general we define the energy norm as

$$E(x) \;=\; \int_0^\infty \mathbf{q}(x)^H M \mathbf{q}(x)\, dz = \int_0^\infty \left[u(x)^2 + v(x)^2 + w(x)^2\right]\, dz, \tag{16}$$

where $M = diag(1, 1, 1, 0)$ represents a weight matrix ensuring that the pressure does not contribute and the superscript H denotes complex conjugate. The results of both methods are in perfect agreement.

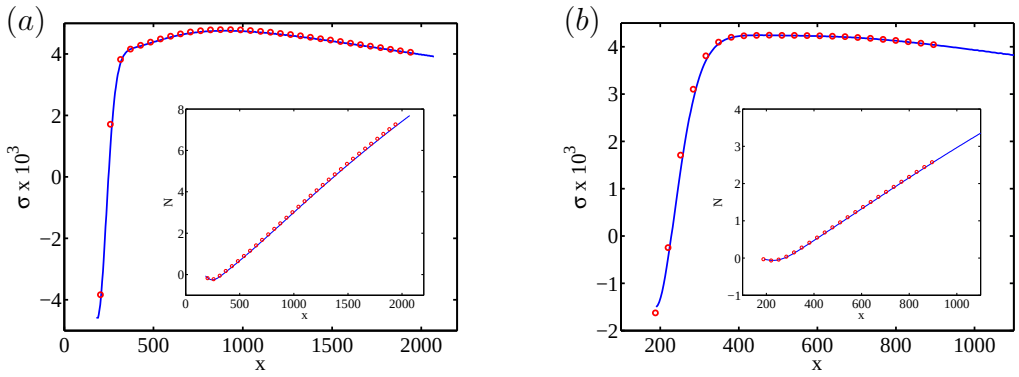

Figure 1: Evolution of crossflow modes in an FSC boundary layer studied by [14] with $\beta_H = 0.333$ and $\Lambda = 45°$ computed by means of the modified PSE (—), and DNS (○). The growth rate σ and the N-Factor are shown for a travelling crossflow mode with (a) $\beta = -0.14$ and $\omega = -0.01$ and (b) a stationary crossflow mode with $\beta = -0.19$. Partly taken from [9].

4 Optimal disturbances

We want to compute the optimal disturbance $\mathbf{q}$ that experiences maximum energy amplification at a specific chordwise position x_1. This means that we want to maximise the objective function $J(\mathbf{q}) = E_1/E_0$ where the subscripts 0 and 1 refer to the initial position and the position of maximum amplification respectively. In order to find the disturbance that maximises $J(\mathbf{q})$ we consider the Lagrange functional

$$\mathcal{L}(\mathbf{q}, \mathbf{q}^\star) = J(\mathbf{q}) - \iint_\Omega (\mathbf{q}^\star)^H \mathbf{L}\mathbf{q} \, dx \, dz. \tag{17}$$

Here, $\mathbf{q}^\star$ is the Lagrange multiplier, also called adjoint variable, and $\Omega = [x_0, x_1] \times [0, \infty]$. The roots of the first variation of (17), which becomes

$$\delta\mathcal{L} = \iint_\Omega (\nabla_{\mathbf{q}^\star}\mathcal{L})^H \delta\mathbf{q}^\star \, dx \, dz + \iint_\Omega (\nabla_{\mathbf{q}}\mathcal{L})^H \delta\mathbf{q} \, dx \, dz, \tag{18}$$

will then represent the optimal disturbance and its corresponding adjoint. $\nabla_{\mathbf{q}}$ denotes a gradient with respect to $\mathbf{q}$. To obtain the roots both inner products in (18) have to render zero independently. Setting the first inner product to zero implies solving (7) such that $\mathbf{L}\mathbf{q} = 0$. The second inner product will be zero if $\nabla_{\mathbf{q}}\mathcal{L} = 0$. This gradient is most easily obtained by adopting the identity

$$\iint_\Omega (\mathbf{q}^\star)^H \mathbf{L}\mathbf{q} \, dx \, dz = \iint_\Omega (\mathbf{L}^\star\mathbf{q}^\star)^H \mathbf{q} \, dx \, dz + \textit{boundary terms} \tag{19}$$

which is derived by employing integration by parts. Rendering the second inner product of (18) zero thus implies solving the so-called *adjoint equations* $\mathbf{L}^\star\mathbf{q}^\star = 0$. The boundary terms in (19) then provide the optimality conditions which relate the solutions of (7) and

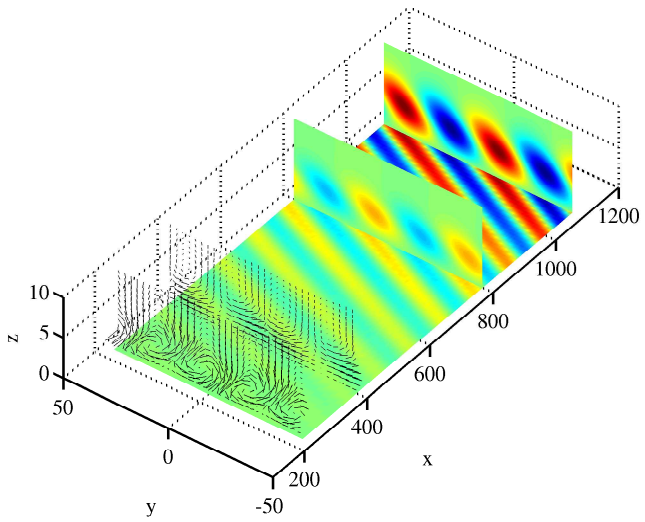

Figure 2: Optimal disturbances with $\beta = -0.14$ and $\omega = -0.01$. Velocity vectors (u, v, w) and coloured planes representing u_ϕ (the velocity component in the direction of the line of constant phase) of the optimal disturbance. Red and blue colours denote positive and negative velocities respectively. For visualisation purposes the horizontal plane which corresponds to $z = 4$ was shifted to $z = 0$.

the adjoint equations at x_0 and x_1 respectively.
The optimality system is practically solved by employing the following iterative procedure. We start by integrating (7) for an arbitrary initial disturbance $\mathbf{q}(x_0)$ where $\alpha(x)$ is determined according to the approach outlined in 3.2.2. At x_1 we obtain the initial adjoint disturbance $\mathbf{q}^\star(x_1)$ as a function of $\mathbf{q}(x_1)$ by employing the optimality condition and then integrate the adjoint equations backward in space from x_1 to x_0. Considering the optimality conditions at x_0 we then obtain a new candidate optimal initial disturbance $\mathbf{q}(x_0)$ as a function of $\mathbf{q}^\star(x_0)$. This procedure is repeated until the energy growth has converged. A more detailed derivation of the optimality system is given in [9].

Figure 2 and figure 3 depict the downstream development of an optimal disturbance whose energy growth is maximised for $x_1 = 2067$. Initially, the disturbance takes the form of vortices which are tilted against the mean crossflow shear. While travelling downstream they rise into an upright position and develop into bended streaks. These in turn evolve into modal crossflow disturbances when entering the *supercritical* domain. This is nicely depicted in figure 3 where the energy growth of both the optimal disturbance and the corresponding modal crossflow disturbance are shown. Further, it becomes clear from figure 3 that non-modal growth is of significant order in three-dimensional boundary layers. The observed optimal growth is more than two orders of magnitude larger than the modal growth of the crossflow disturbance in this case. Combining these observations we can conclude that non-modal growth is the result of two different physical effects. The first one is the well-known *lift-up effect* where streamwise vortices produce streaky

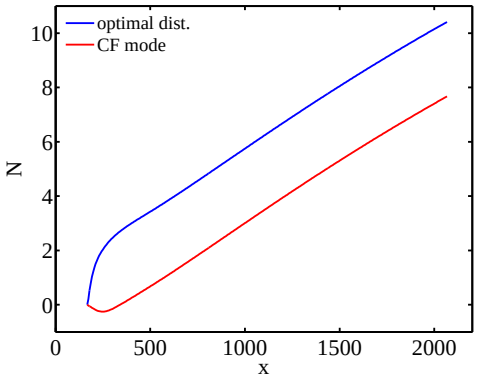

Figure 3: N-factor of both the optimal disturbance and the corresponding crossflow mode with $x_0 = 167$, $x_1 = 2067$, $\beta = -0.14$ and $\omega = -0.01$ obtained by solving the modified PSE.

structures by displacing fluid particles vertically which keep their horizontal momentum. The second effect is the *Orr-mechanism* where tilted vortices extract energy from the meanflow while being erected.

5 Receptivity

Modelling the receptivity process means to describe the initiation of boundary layer instabilities such as crossflow disturbances. In this section we develop two approaches that provide initial amplitudes of crossflow modes in a boundary layer which is exposed to free-stream vorticity. The latter is considered to be a good basis for modelling free-stream turbulence. The first approach approximates initial amplitudes by projecting free-stream disturbances onto the formerly obtained optimal disturbances. The second approach is based on a direct solution of the modified PSE for initial vortical free-stream disturbances. Eigenfunctions associated with the continuous spectrum of the Orr-Sommerfeld (OS) equation are used to represent unsteady vortical free-stream disturbances. They have been used for similar purposes by [14]. These, so called, continuous modes are oscillatory in the free-stream and damped toward the wall. In the free-stream the Orr-Sommerfeld equation simplifies to a homogeneous ordinary differential equation of the form

$$(\mathcal{D}^2 - \alpha^2 - \beta^2)^2 w - iRe(\alpha U_\infty + \beta V_\infty - \omega)(\mathcal{D}^2 - \alpha^2 - \beta^2)w = 0 \tag{20}$$

and an analytical dispersion relation is obtained which reads

$$\alpha = \frac{1}{2} i \left(\sqrt{(ReU_\infty)^2 + 4(iRe(\beta V_\infty - \omega) + \beta^2 + \gamma^2)} - ReU_\infty \right). \tag{21}$$

Here, the wall-normal wavenumber is denoted by γ and $\mathcal{D} = \partial/\partial z$. Using the dispersion relation (21) and a boundedness condition in the free-stream the eigenfunction of the continuous OS-mode can be determined numerically. For details the reader is referred to [14]. An example of such an eigenfunction in a Falkner-Skan-Cooke boundary layer is

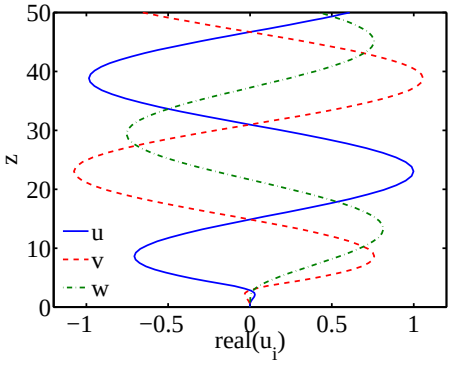

Figure 4: Shape functions of u, v and w of a continuous spectrum eigenmode of the Orr-Sommerfeld equation in a Falkner-Skan-Cooke boundary layer for $\gamma = 0.126$, $x = 167$, $\beta = -0.14$ and $\omega = -0.01$.

shown in figure 4. Note that a full representation of free-stream vorticity would also require a solution to the Squire equations which represents the wall-normal vorticity component. However, as outlined in [14] the Orr-Sommerfeld and Squire solutions evolve independently upstream of the leading edge if the incoming turbulent flow is homogeneous and isotropic. The coupling between the two solutions is a slow viscous process which is initiated at the leading edge. Hence, the shape of the OS solution a short distance downstream of the leading edge is barely affected by the coupling.
In the following we quantify receptivity, i.e. the initial amplification of crossflow modes, by determining receptivity coefficients. A receptivity coefficient $C_V = C_V(\beta, \omega, \gamma, x_0)$ is defined according to

$$C_V = \frac{A_R}{\epsilon_v}. \tag{22}$$

A_R denotes the receptivity amplitude, i.e. the equivalent amplitude the excited pure crossflow mode must have at the initial position in order to finally attain the same amplitude as the boundary layer disturbance which evolves as a response to free-stream modes. ϵ_v denotes the maximum amplitude of the vortical free-stream mode. Both amplitudes are determined as the wall-normal maximum of u_{rms}.

5.1 Projection onto optimal disturbances

The fact that optimal disturbances take the form of vortices initially and develop into modal disturbances further downstream suggests to project vortical disturbances to optimal ones at some initial position x_0. In this way, response amplitudes for modal crossflow instabilities and the corresponding receptivity coefficients are approximated.
Hence, for each vortical free-stream disturbance with parameters $(x_0, \beta, \omega, \gamma)$ the respective optimal disturbance $\mathbf{q}_{opt}(\omega, \beta)$ is computed. Then the free-stream disturbance $\mathbf{q}(x_0)$

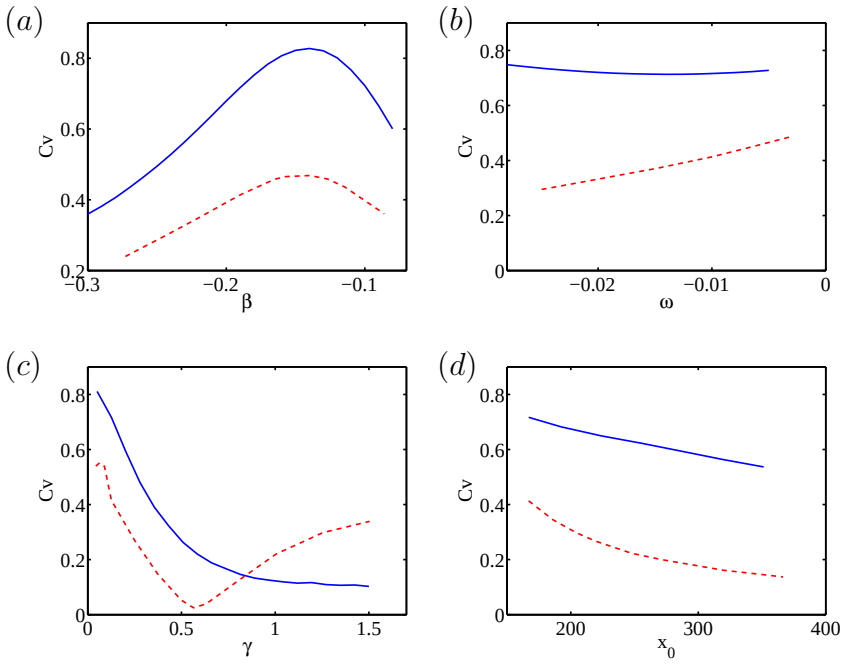

Figure 5: Dependence of the receptivity coefficient C_V on (a) the spanwise wavenumber β, (b) the wall-normal wavenumber γ, (c) the frequency ω and (d) the initial position x_0. Comparison between results obtained by projecting vortical free-stream disturbances to optimal disturbances (—) and the DNS of [14](---). Parameters $(x_0, \beta, \omega, \gamma) = (167, -0.19, -0.01, 0.126)$ represent the basis from which individual parameters are varied.

is projected to the optimal disturbance $\mathbf{q}_{opt}(x_0)$ employing the energy inner product

$$c_{pr} = \frac{\int_0^\infty \mathbf{q}(x_0)^H M \mathbf{q}_{opt}(x_0)\, dz}{\int_0^\infty \mathbf{q}_{opt}(x_0)^H M \mathbf{q}_{opt}(x_0)\, dz}, \tag{23}$$

where c_{pr} denotes the projection coefficient. The approximate response of the boundary layer is then given by the disturbance

$$\mathbf{q}_{pr} = c_{pr} \mathbf{q}_{opt}. \tag{24}$$

Receptivity coefficients obtained by using this projection technique are presented in figure 5 and compared to those [14] obtained by employing DNS. For this parametric study the parameters $(x_0, \beta, \omega, \gamma) = (167, -0.19, -0.01, 0.126)$ are taken as a basis from which each individual parameter is varied. We obtain a reasonable agreement to the DNS results. The order of magnitude of the receptivity coefficients is correctly predicted and similar trends as those observed from DNS are reproduced. Considering figure 5 (a) the

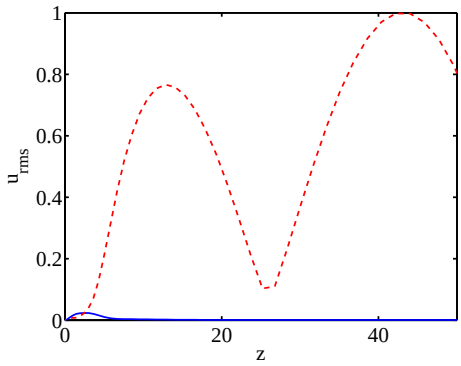

Figure 6: Comparison between the vortical free-stream disturbance (---) and the initial disturbance $\mathbf{q}_{pr}(x_0)$ obtained through projection (—). $x_0 = 167$, $\omega = -0.01$, $\beta = -0.19$ and $\gamma = 0.126$

same spanwise wavenumber β yielding maximum receptivity as in the DNS simulations is obtained. Also, C_V decreases with increasing x_0 as becomes apparent from figure 5 (d). Further, the initial decay of C_V with respect to γ is reproduced by the projection procedure. The largest discrepancies are obtained for low values of ω and for high values of γ. However, the free-stream modes of high γ which [14] found to deeply penetrate into the boundary layer might in practice be irrelevant. This is due to the fact that the turbulent kinetic energy of turbulent flow fields is usually concentrated at small wavenumbers. Since the magnitudes of the here computed receptivity coefficients are generally higher than the DNS results we can conclude that the projection technique provides predictions which are on the "safe side".
By comparing the initial disturbance $\mathbf{q}_{pr}(x_0)$ resulting from the projection to the initial vortical free-stream disturbance (see figure 6) it becomes clear how the performance of this technique might be improved. The comparison shows that a single optimal disturbance constitutes a rather incomplete basis for representing vortical free-stream disturbances in form of continuous OS modes. The projection coefficient becomes very small and the resulting initial disturbance does not reflect the shape of the free-stream mode correctly. Enlarging the basis by computing an additional number of orthogonal basis functions would probably improve the performance of this approach. Such orthogonal eigenfunctions are not straightforward to obtain though since three-dimensional boundary layers are very unstable. Methods based on projecting out existing basis functions, i.e. Gram-Schmidt or Arnoldi, are difficult to employ because any numerical noise will again lead to the optimal disturbance and the resulting new orthogonal basis function will be zero.

5.2 Directly solving the modified PSE

The evolution of crossflow modes predicted by the modified PSE is in excellent agreement with DNS results as is shown by [9] (see also figure 1). Figure 7 (a) shows that

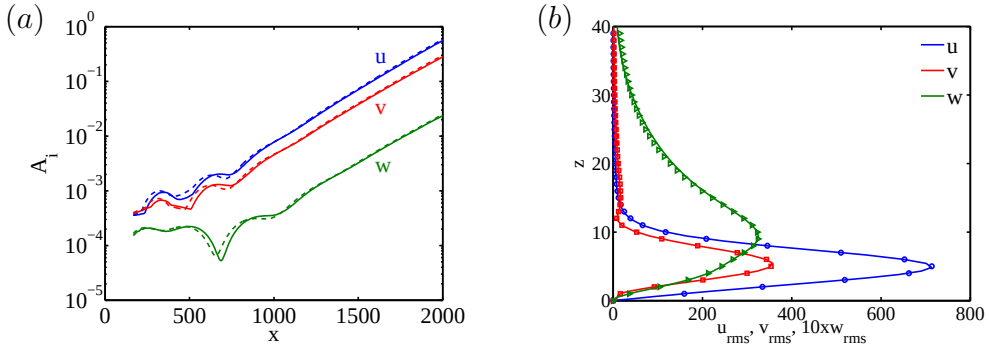

Figure 7: (a) Spatial evolution of the boundary layer disturbance excited by a continuous Orr-Sommerfeld mode with $\gamma = 0.126$, $\beta = -0.14$ and $\omega = -0.01$. Comparison between DNS (---) and PSE (—) results where the modified PSE was employed. A_i denotes the wall-normal maximum of the disturbance velocity components u_{rms}, v_{rms} and w_{rms} respectively. (b) Comparison between the disturbance profiles of the boundary layer response (—) and the shape functions of a pure crossflow mode (symbols) at the last station $x = 2067$. u (○), v (□) and w (▷) are shown.

also the boundary layer response to free-stream vorticity is almost perfectly predicted by the modified PSE. Here, the continuous Orr-Sommerfeld mode presented in figure 4 is introduced at $x_0 = 167$ and the downstream evolution of the disturbance is computed employing the modified PSE. A comparison of the computed boundary layer response to the DNS results by [14] shows that even the initial transient part is well described by the modified PSE. Hence, the amplitude of the excited crossflow mode is predicted correctly. Figure 7 (b) compares the boundary layer response at the final position to the shape functions of a pure crossflow mode. The perfect agreement shows that the excited boundary layer disturbance has developed into a crossflow mode. This exemplifies a direct receptivity mechanism where the excited boundary layer disturbance experiences non-modal growth initially and evolves into a crossflow mode further downstream.

We again perform the same parametric study that was conducted by [14]. The results are shown in figure 8. In general the comparison between the results of the modified PSE and DNS is very good. The values of C_V are similar and the trends observed from the DNS results are also predicted by the modified PSE. Figure 8 (a) shows that maximum receptivity is obtained for $\beta = -0.15$. The receptivity with respect to frequency presented in figure 8 (b) increases for smaller moduli of ω. The largest differences between results from modified PSE and DNS are again observed for high values of γ as can be seen in figure 8 (c). For lower values of γ receptivity coefficients obtained from both methods are very similar showing that receptivity is most efficient at large wall-normal length scales. Also the general trends, i.e. a minimal receptivity coefficient for intermediate scales as well as increasing coefficients for higher values of γ are apparent from the solutions of the modified PSE. As discussed before, the free-stream modes of high γ which are predicted worst by the modified PSE might be irrelevant in praxis. Finally, figure 8 (d) reveals that

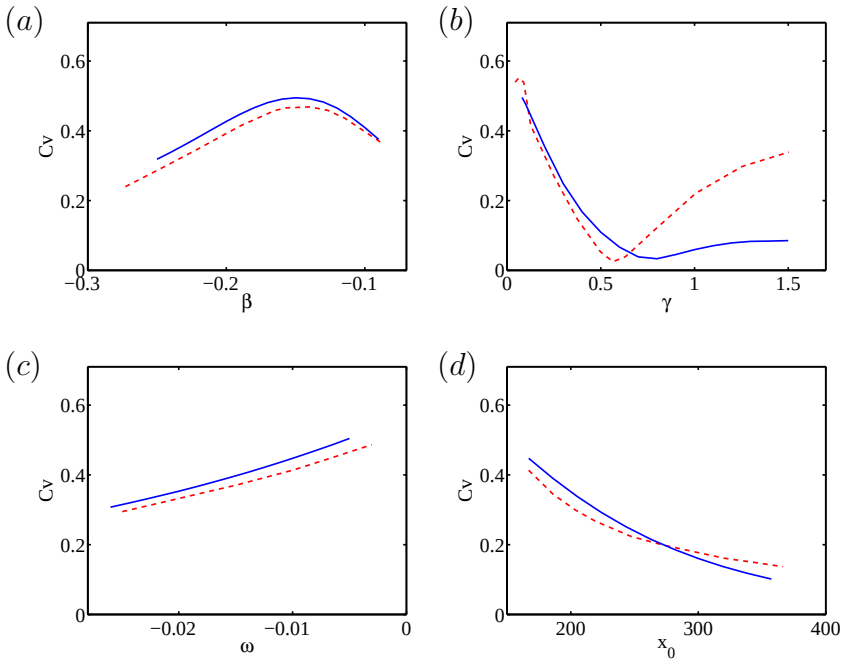

Figure 8: Dependence of receptivity coefficients C_V on (a) the spanwise wavenumber β, (b) the wall-normal wavenumber γ, (c) the frequency ω and (d) the initial position x_0. Comparison between the solution of the modified PSE (—) and the DNS results by [14] (---). Parameters $(x_0, \beta, \omega, \gamma) = (167, -0.19, -0.01, 0.126)$ represent the basis from which individual parameters are varied.

also the dependence of receptivity with respect to the position of inception is predicted correctly by the modified PSE.
The small differences between results from DNS and modified PSE which generally become apparent from figure 8 may be due to several reasons. One reason is that [14] employ a fully spectral DNS code which builds on a Fourier representation along the chordwise direction. The required chordwise periodicity is obtained by using a fringe region where the vortical free-stream modes are introduced. The receptivity process might thus already have been initiated before the disturbance passes the position of inception x_0. Another small error may be introduced by the PSE approximation.

6 Conclusions & Outlook

A new method has been presented which was introduced by [9] and which represents a modification of the well-known PSE. These modified PSE allow to efficiently predict the evolution of both modal and non-modal disturbances in three-dimensional boundary layers and are therefore perfectly suited to study optimal disturbances and receptivity.
We computed optimal disturbances and showed that three-dimensional boundary layers have a significant potential for non-modal growth. Since optimal disturbances take the form of vortices initially and evolve into crossflow modes further downstream we conclude that non-modal growth initiates modal disturbances. It is therefore related to a receptivity mechanism.
Two methods have been developed which determine the response of three-dimensional boundary layers to free-stream vorticity. Eigenmodes of the continuous spectrum of the Orr-Sommerfeld equation have been used to model free-stream vorticity.
The first method which provides an approximation of the boundary layer response by projecting vortical free-stream disturbances to optimal ones yields reasonable results. The obtained receptivity coefficients are of the correct order of magnitude and several trends can be reproduced. The advantage of this method is that optimal disturbances need to be computed only once. The response to different free-stream disturbances is then obtained very efficiently by projection.
The second method determines the boundary layer response by directly solving the modified PSE where the vortical free-stream disturbances are taken as initial disturbances. The performance of this method is remarkable. The agreement to DNS results is very good for almost the whole parameter space. In particular, it should be noted that the modified PSE provide results at a small fraction of the time required for direct numerical simulations. Hence, the modified PSE represent a suitable tool for the analysis of receptivity in three-dimensional boundary layers.

Future work will focus on developing models to determine the response of the boundary layer to free-stream turbulence. A possible approach would be to connect initial direct numerical simulations to the linear modified PSE. Furthermore it is easy to extend the modified PSE such that effects of compressibility and wall curvature can be accounted for. Hence, performing parametric studies of receptivity for compressible boundary layers

on curved walls would represent another interesting continuation.

7 Acknowledgements

The authors would like to thank Lars-Uve Schrader and Luca Brandt for providing data and for related discussions. This work has been supported by the European Commission through the FP6 project "TELFONA" (Contract No AST4-CT-2005-516109).

REFERENCES

[1] H. Deyhle and H. Bippes, Disturbance growth in an unstable three-dimensional boundary layer and its depence on environmental conditions, *J. Fluid Mech.*, **316**, 73–113 (1996).

[2] H. Bippes, Basic experiments on transition in three-dimensional boundary layers dominated by crossflow instability, *Progress in Aerospace Sciences*, **35**, 363–412 (1999).

[3] L. U. Schrader, S. Amin and L. Brandt, Transition to turbulence in the boundary layer over a smooth and rough swept plate exposed to free-stream turbulence, *J. Fluid Mech.*, **646**, 297–325 (2010).

[4] A. Bottaro, A receptive boundary layer, *J. Fluid Mech.*, **646**, 1–4 (2010).

[5] K. M. Butler and B. F. Farrell, Three-dimensional optimal perturbations in viscous shear flow, *Phys. Fluids*, **4**, 1637–1650 (1992).

[6] S. C. Reddy and D. S. Henningson, Energy growth in viscous channel flow, *J. Fluid Mech.*, **252**, 209–238 (1993).

[7] P. Andersson, M. B. Berggren and D. S. Henningson, Optimal disturbances and bypass transition in boundary layers, *Phys. Fluids*, **11**, 134–150 (1999).

[8] P. Luchini, Reynolds-number-independent instability of the boundary layer over a flat surface: optimal perturbations, *J. Fluid Mech.*, **404**, 289–309 (2000).

[9] D. Tempelmann, A. Hanifi and D. S. Henningson, Spatial optimal growth in three-dimensional boundary layers, *J. Fluid Mech.*, **646**, 5–37, (2010).

[10] K. S. Breuer and T. Kuraishi, Transient growth in two- and three-dimensional boundary layers, *Phys. Fluids*, **6(6)**, 1983–1993 (1994).

[11] P. Corbett and A. Bottaro, Optimal linear growth in swept boundary layers, *J. Fluid Mech.*, **435**, 1–23 (2001).

[12] F. P. Bertolotti, Response of the Blasius boundary layer to free-stream vorticity, *Phys. Fluids*, **9**, 2286–2299 (1997).

[13] L. Brandt, D. S. Henningson and D. Ponziani, Weakly non-linear analysis of boundary layer receptivity to free-stream disturbances, *Phys. Fluids*, **14**, 1426–1441 (2002).

[14] L. U. Schrader, L. Brandt and D. S. Henningson, Receptivity mechanisms in three-dimensional boundary layer flows, *J. Fluid Mech.*, **618**, 209–241(2009).

[15] F. P. Bertolotti, T. Herbert and P. R. Spalart, Linear and nonlinear stability of the Blasius boundary layer, *J. Fluid Mech.*, **242**, 441–474 (1992).

[16] M. Simen, Local and Non-local Stability Theory of Spatially Varying Flows, In *Instability, Transition and Turbulence* (ed. M. Y. Hussaini, A. Kumar & C. L. Streett), 181–195 (1992), Springer.

[17] O. Levin and D. S. Henningson, Exponential vs Algebraic Growth and Transition Prediction in Boundary Layer Flow, *Flow, Turbulence and Combustion*, **70**, 183–210 (2003)

[18] S. Bagheri and A. Hanifi, The stabilizing effect of streaks on Tollmien-Schlichting and oblique waves: A parametric study, *Phys. Fluids*, **19**, (2007)

[19] F. Li and M.R. Malik, On the Nature of the PSE Approximation, *Theoretical and Computational Fluid Dynamics*, **8**, 253–273 (1996).

[20] H. Haj-Hariri, Characteristics Analysis of the Parabolized Stability Equations, *Studies in Applied Mathematics*, **92**, 41–53 (1994)